

Simultaneous deorientation and lifetime measurement in ^{98}Ru using the recoil distance Doppler shift method in inverse Coulomb excitation

D. Radeck,^{1,2,*} V. Werner,¹ G. Ilie,^{1,3} N. Cooper,¹ V. Anagnostatou,^{1,4} T. Ahn,¹ L. Bettermann,^{1,2} R. J. Casperson,¹ R. Chevrier,^{1,5} A. Heinz,¹ J. Jolie,² D. McCarthy,^{1,4} M. K. Smith,¹ and E. Williams¹

¹WNSL, Yale University, New Haven, Connecticut, USA

²Institut für Kernphysik, Universität zu Köln, Köln, Germany

³National Institute for Physics and Nuclear Engineering, Bucharest, Romania

⁴Department of Nuclear Physics, University of Surrey, Guildford, United Kingdom

⁵Department of Nuclear Physics, University of Caen Basse Normandie, F-14000 Caen, France

(Received 4 June 2011; revised manuscript received 24 October 2011; published 3 January 2012)

We measured the lifetimes of the $2_{1,2}^+$ and 4_1^+ states in ^{98}Ru in order to reduce their uncertainties and resolve the discrepancies in the literature for the lifetime of the 4_1^+ state. Coulomb excitation in inverse kinematics was used to populate excited states in ^{98}Ru , and the recoil distance doppler shift (RDDS) method was employed using the nNew Yale plunger device (NYPD). This technique combined with inverse Coulomb excitation requires several corrections due to relativistic and deorientation effects but yields high precision lifetimes. The determined $B_{4/2} = B(4_1^+ \rightarrow 2_1^+)/B(2_1^+ \rightarrow 0_1^+) = 1.86(16)$ agrees well with the vibrational limit. In order to analyze the data, a new method for the deorientation correction of RDDS data was developed using the perturbation of experimental angular correlations. The simultaneous measurement of deorientation and lifetime of a given state and its application are discussed. The method is suitable for radioactive beam experiments.

DOI: [10.1103/PhysRevC.85.014301](https://doi.org/10.1103/PhysRevC.85.014301)

PACS number(s): 21.10.Tg, 21.60.Ev, 23.20.En, 25.70.De

I. INTRODUCTION

For understanding the evolution of nuclear structure within an isotopic chain or mass region, e.g., for global fits in collective as well as in microscopic models, an accurate knowledge of basic data is necessary. In particular, for predicting values in regions far away from the stability line, precision measurements of accessible nuclei must be available in order to constrain nuclear models.

The $B_{4/2}$ value corresponding to the ratio between the $E2$ transition strengths of the $4_1^+ \rightarrow 2_1^+$ and the $2_1^+ \rightarrow 0_1^+$ transition [$B_{4/2} = B(E2; 4_1^+ \rightarrow 2_1^+)/B(E2; 2_1^+ \rightarrow 0_1^+)$], like its energetic analog, the $R_{4/2}$ value [$R_{4/2} = E(4_1^+)/E(2_1^+)$], is sensitive to the collective nature of the low-energy excitations. In the geometrical limit, $B_{4/2} = 2$ corresponds to a vibrational nucleus, $B_{4/2} = 1.43$ to a rotor, and for a magic nucleus one expects $B_{4/2} < 1$. Deviations from these values in the limits of other collective models occur due to the finite size of the model space; e.g., within the $U(5)$ limit [1] of the algebraical interacting boson model (IBM) [2], $B_{4/2}$ in a vibrational nucleus with $N = 4$ valence bosons takes the value 1.5 instead of 2. Also, due to the transitional character of real nuclei, measured values are expected to lie between these limits. Nuclei near the $N = 50$ shell closure form an interesting region to investigate how proton-neutron collectivity evolves from near-spherical into deformed nuclei. Much theoretical work focuses on the light Ru and Pd isotopes with $N > 50$, e.g., Refs. [3–6].

One particular example in which conflicting lifetime measurements [7,8] have prompted debate is ^{98}Ru , as discussed in Refs. [9,10]. In Ref. [9], a breakdown of vibrational symmetry

in ^{98}Ru was observed due to two phenomena: the expected vibrational structure fails for states above the two-phonon triplet, and the $B_{4/2}$ value of $B_{4/2} < 1$ published in [8] is untypical for a nonmagic nucleus. For ^{98}Ru , a weak-collective or vibrational $B_{4/2}$ value is expected due to its proximity to the $N = 50$ shell closure. A remeasurement of lifetimes using inverse Coulomb excitation [10] clarified the situation of the noncollective $B_{4/2}$ value but resulted in a large uncertainty of the $B(E2; 4_1^+ \rightarrow 2_1^+)$ value since it was measured relative to the $B(E2; 2_2^+ \rightarrow 2_1^+)$ value. Due to the unknown strength of the $2_2^+ \rightarrow 0_2^+$ transition, two assumptions were made to determine this value resulting in two possible $B_{4/2}$ ratios. The present literature values for ^{98}Ru are summarized in Fig. 1 underlining the contradictory possible interpretations. Nuclear structure considerations suggest that the most precise value [8] may not be correct and the conflict with the result from [7] needs to be resolved. The most recent measurement [10] agrees with [7], however, has large statistical errors. Hence, a structural interpretation of ^{98}Ru is difficult due to the lack of accurate data for essential values such as the transition strengths among the lowest-lying states.

To investigate the disagreement in the literature and to obtain more precise values for the transition strengths in ^{98}Ru , a measurement of lifetimes for the $2_{1,2}^+$ and 4_1^+ states in this nucleus was performed at the Wright Nuclear Structure Laboratory, Yale University. The measurement employed an experimental approach developed in recent years, described in [11,12], that combines safe Coulomb excitation in inverse kinematics with the well-established recoil distance doppler shift (RDDS) method [13]. With this technique, one obtains almost background-free spectra. As a result of the relatively high velocity of the excited nuclei, the shifted and unshifted components of the transition of interest are easily separable

*radeck@ikp.uni-koeln.de

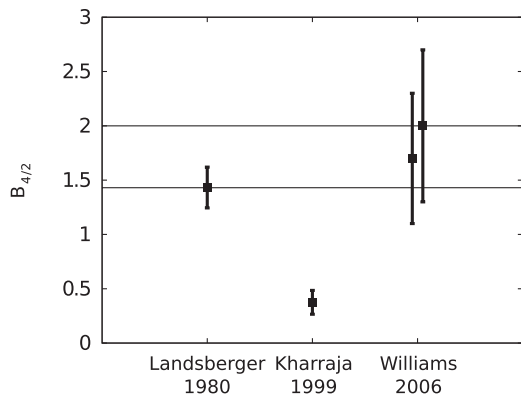


FIG. 1. The results of previous measurements for the $B_{4/2}$ value of ^{98}Ru (Landsberger1980 [7], Kharraja1999 [8], Williams2006 [10]). For comparison, the geometrical limits for vibrator ($B_{4/2} = 2$) and rotor ($B_{4/2} = 1.43$) are shown as well.

at large angles. Inverse Coulomb excitation was chosen to populate ^{98}Ru because a fusion evaporation reaction with a sufficiently large v/c value is difficult and due to the low abundance of the isotope, measurements in direct kinematics are not practical.

In addition to this work, a $\gamma\gamma$ angular correlation experiment was performed at the University of Cologne using the HORUS setup [14,15] and the $^{99}\text{Mo}(^3\text{He}, 2n)$ reaction to populate low-spin states in ^{98}Ru . With this data, we plan to clarify discrepancies in earlier measurements regarding the spin of various low-energy states and shed light on the characteristics of low-spin states by determining multipole mixing ratios. The results will be discussed in a forthcoming publication [16].

A second focus of this publication is the deorientation effect due to the hyperfine interaction and its consequences on plunger measurements as was discussed in [17–19]. In experiments employing the differential doppler shift method [20,21] with small v/c , sufficiently small lifetimes, and coincidence data, no correction for deorientation is necessary [22]. In the present experiment, the deorientation effect is clearly visible for the first 2_1^+ state. The correction performed by measuring the deorientation via the perturbed angular correlations is derived and is discussed in Sec. IV. The method is based on phenomenological approaches from [23–25]. The present setup and reaction allow simultaneous lifetime and deorientation measurements. Due to the magnetic character of the hyperfine interaction, the method can also be used to extract relative g factors in isotopic chains from inverse kinematics experiments, and is therefore especially suitable for use with radioactive ion beams. Recently, integral attenuation factors have been measured and used to determine g factors using radioactive ion beams [26]. The measurement of differential attenuation coefficients using a plunger setup has the advantage to measure lifetimes using the RDDS method and g factors simultaneously provided that calibration data exists.

In Sec. II, the performed experiment is presented, in Sec. III, the RDDS method in combination with inverse Coulomb excitation is discussed. Section IV focuses on nuclear deorientation and the correction of the measured lifetimes for

this effect. The results of the lifetime analysis are presented in Sec. V and discussed in Sec. VI.

II. EXPERIMENT

To populate excited states in ^{98}Ru , we used Coulomb excitation in inverse kinematics. The ^{98}Ru beam was provided by the ESTU Tandem accelerator at the Wright Nuclear Structure Laboratory at Yale University and impinged on a ^{24}Mg target. A beam energy of $E_{\text{beam}} = 300$ MeV was chosen, well below the Coulomb barrier of $E_{\text{coul}} = 347$ MeV. The average beam current was $I = 2.5$ enA at a charge state of $q = 16^+$. The ^{24}Mg target had a thickness of 0.7 mg/cm 2 and the stopper consisted of $^{\text{nat}}\text{Cu}$ with a thickness of 15.7 mg/cm 2 . The new Yale plunger device (NYPD) [27] was used and target-to-stopper distances ranging from 3 μm to 450 μm were measured.

The γ rays were detected using the detector array SPEEDY [28] with ten HPGe Clover detectors of the YRAST ball array [29]. Four Compton-shielded detectors were mounted at both backward and forward angles, and two nonshielded detectors were positioned at 90 degrees with respect to the beam axis. Since each Clover detector can be split into two pairs of crystals at the same polar angle relative to the beam axis, the setup leads to six groups of detectors, or rings, in the analysis at angles of 36.5° (ring 1), 46.5° (ring 2), 85° (ring 3), 95° (ring 4), 133.5° (ring 5), and 143.5° (ring 6). The setup is shown in Fig. 2. The mean velocity of the excited ^{98}Ru nuclei was $4.50(6)\%c$, measured from the Doppler-shift using the centroid of the shifted component. Due to the setup geometry and large recoil velocity, the γ rays of interest had two clearly separable components: an unshifted component originating from nuclei emitting at rest in the stopper foil, and a shifted component due to the Doppler shift when emitted in-flight between target and

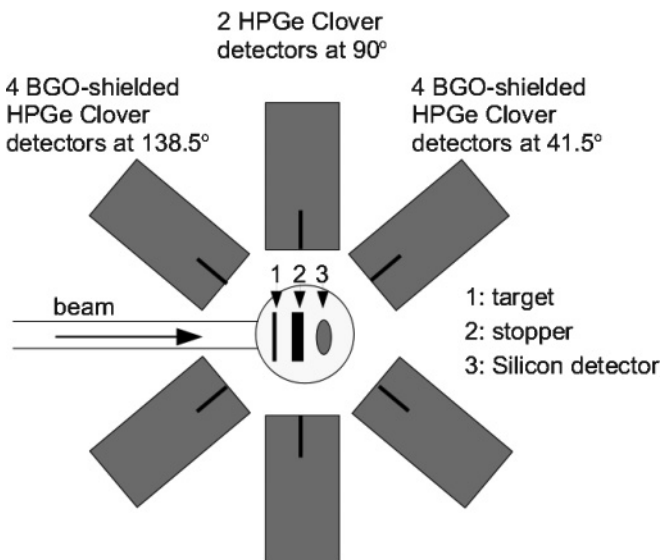


FIG. 2. A schematic view of the setup. In the center the target chamber is shown with target and stopper foil and the Si detector at 0° . The chamber is surrounded by ten clover detectors. The beam is coming from the left.

stopper. In addition, a tail of the unshifted peak was visible, due to nuclei emitting γ rays while slowing down in the stopper foil.

After the reaction, the forward-scattered ^{24}Mg nuclei passed the stopper foil and were detected in a silicon detector that was mounted inside the target chamber at 0 degrees, as shown in Fig. 2. The particle detector covered a half angle of 29.7 to 28.3 degrees in the laboratory frame, depending on the distance between both foils, i.e., the target position. Data were taken using the following triggers: particle- γ coincidence, downscaled γ -singles, and downscaled particle-singles events.

III. THE RECOIL DISTANCE DOPPLER SHIFT METHOD USING PROJECTILE COULOMB EXCITATION

The RDDS method [13] is a well-established tool to measure lifetimes in the ps range. The lifetime of a level is deduced from analyzing the differences in intensities of shifted and unshifted peak as a function of the distance between target and stopper. This distance influences the probability of in-flight decay. The RDDS technique is model independent, in contrast to relative measurements of matrix elements using Coulomb excitation alone. For small or medium beam energies, nuclear levels are strongly populated by direct Coulomb excitation and feeding intensity from higher levels is often negligible. Thus, using Coulomb excitation as the excitation mechanism has the advantage that unobserved side feeding as in fusion evaporation reactions does not appear. This an important aspect of lifetime analyses. By using the particle- γ trigger, we ensure that the nuclei of interest were Coulomb excited in the target material and not in the stopper. Using this trigger also yields almost background-free spectra. In Fig. 3, the $2_1^+ \rightarrow 0_1^+$ transition [Figs. 3(a) and 3(b)] and the $4_1^+ \rightarrow 2_1^+$ and $2_2^+ \rightarrow 2_1^+$ transitions [Figs. 3(c) and 3(d)] are shown for one ring and two limiting distances labeled relative to electrical contact of the foils.

While recoil velocities in traditional RDDS experiments are typically $v/c = 0.5\text{--}3\%$, inverse reactions lead to much higher velocities of the nuclei of interest. Thus, the shifted and unshifted components of a transition are well separated; this separation allows for a precise determination of the intensities. However, a tail due to the de-exciting nuclei that are not completely at rest but slowing down in the stopper material has to be added into the intensity of the unshifted component. The high recoil velocity requires corrections due to relativistic effects, differences in the efficiency of shifted and unshifted components, and a correction due to the time- and thus distance-dependent alignment of the nucleus.

The relativistic solid-angle correction (Lorentz boost) was calculated using the equation [30]

$$\frac{d(\Omega_\gamma)}{d(\Omega'_\gamma)} = \left(1 + \frac{\Delta E_\gamma}{E_{\gamma_0}}\right)^2, \quad (1)$$

with $\Delta E_\gamma = E_\gamma - E_{\gamma_0}$, E_γ the Doppler-shifted transition energy, E_{γ_0} the unshifted energy of the transition, Ω_γ the solid angle in the rest coordinate system and Ω'_γ the solid angle in the laboratory system. By this means, correction factors for the shifted components were determined for each ring. The

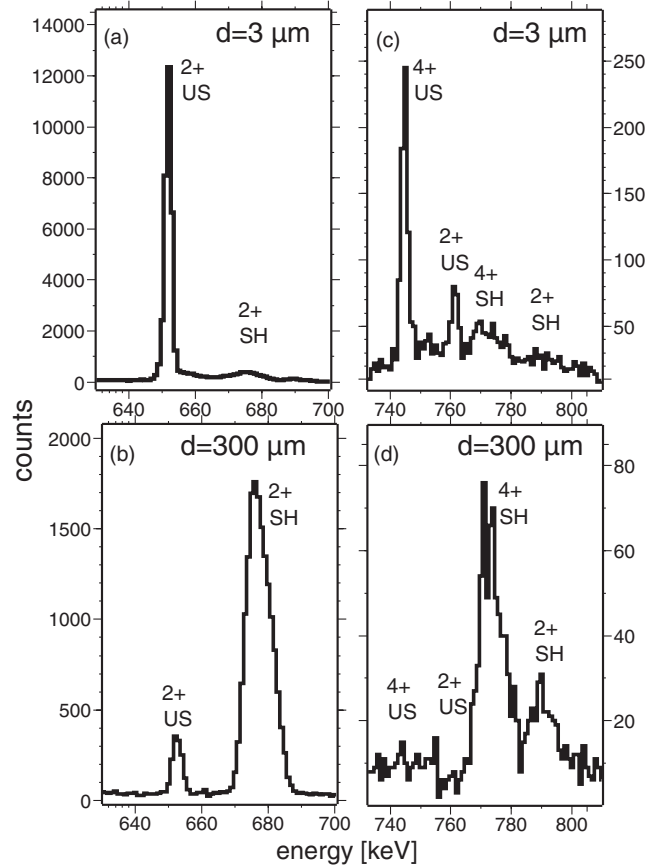


FIG. 3. Spectra for the $2_1^+ \rightarrow 0_1^+$ transition at $E_\gamma = 652$ keV [(a) and (b)] and for the $4_1^+ \rightarrow 2_1^+$ transition at $E_\gamma = 745$ keV and $2_2^+ \rightarrow 2_1^+$ transition at $E_\gamma = 761$ keV [(c) and (d)] for two limiting distances $d = 3 \mu\text{m}$ and $d = 300 \mu\text{m}$ at forward angles (ring 1). The components are labeled “US” for the unshifted component emitted at rest in the stopper foil and “SH” for the shifted component emitted in-flight between target and stopper foil.

necessary correction for the deorientation effect is discussed in detail in the following section.

IV. DEORIENTATION EFFECT

After Coulomb excitation at the target, the nuclei of interest are highly aligned. This alignment leads to an anisotropy of emitted γ radiation. During recoil into vacuum, the alignment diminishes with time. In consequence, the emitted γ radiation has a time-dependent angular distribution. This is the so-called deorientation effect.

The deorientation occurs due to the hyperfine interaction between the nuclear spin \vec{I} and the spin of the electrons \vec{J} . The alignment is equivalent to an oriented nuclear spin \vec{I} . This spin couples to the randomly oriented spin of the electron configuration \vec{J} . In consequence, the nuclear spin \vec{I} precesses around the total angular momentum $\vec{F} = \vec{I} + \vec{J}$ which is conserved for the free ion system, as shown in Fig. 4. This precession around the direction of \vec{F} leads to a loss of alignment with time.

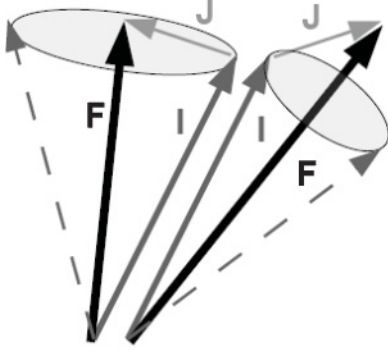


FIG. 4. Schematic drawing of the resulting orientation of \vec{F} and the precession of \vec{I} around \vec{F} depending on the orientation of \vec{J} (figure adopted from [24]).

In our experiment, detecting the scattered ^{24}Mg nuclei at 0° corresponds to a dominant population of $m = 0$ substates in the excited ^{98}Ru nuclei, where the quantization axis is given by the beam direction. Since time is equivalent to distance in plunger experiments, the time-dependent alignment leads to a distance-dependent angular correlation. Changing the distance is equivalent to varying the interaction time. As will be shown, the distance-dependent angular correlation is different for unshifted and shifted components; thus, the effect needs to be taken into account when the intensities of both components are compared for lifetime determinations.

One observable that clearly tests whether the experiment was sensitive to the deorientation of a specific state is the normalized sum of unshifted and shifted component of the transition. After correction for efficiency and the solid angle of the particle detector, this sum has to be constant when no deorientation is present. Normalization is necessary due to the varying measurement times for each distance and variations in beam intensity and was done using particle singles rates as a reference. The corrected intensities of the shifted and unshifted component are shown in Fig. 5 for the ring at 36.5° . The deorientation effect is visible since the total number of counts is not constant but shows a clear drop, i.e., it depends on distance. Another experimentally accessible observable is the ratio between the intensities of the same component at 90 degrees and at forward angles. Therein, the effect of varying angular correlations is clearly seen, if a sensitivity to the deorientation effect is present. This is shown in Fig. 6 for all three populated states. The effect is clearly visible for the 2_1^+ state while it is not observable within the error for the 4_1^+ and 2_2^+ states.

Progress has been made in describing the hyperfine interaction theoretically. Recently, first *a priori* calculations of integral attenuation factors were published [31]. The results are promising and have the major advantage that calibrations with isotopes having well-known properties become unnecessary. However, to date, the predictive power of such calculations has not been tested and systems of heavy ions with a distribution of charge states [32] remain a challenge for theoretical treatment, since the time evolution of the electronic system is difficult to model. In consequence, we measured the deorientation effect directly and used phenomenological models to describe the

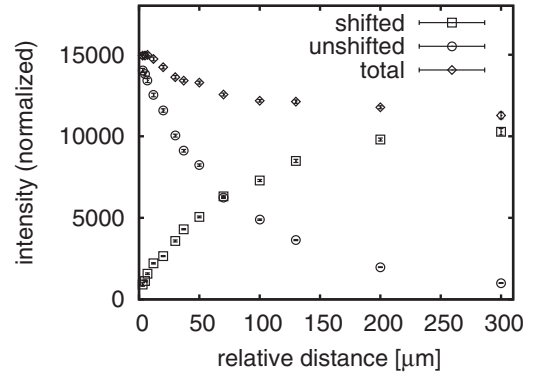


FIG. 5. The intensities at $\Theta = 36.5^\circ$ (ring 1) of the shifted (\square) and unshifted (\circ) components of the $2_1^+ \rightarrow 0_1^+$ transition and the total number of counts $I^{\text{total}} = I^{\text{SH}} + I^{\text{US}}$ (\diamond) after applying all required corrections except for the correction for deorientation.

results. Investigations ([24] and references therein) show an approximately exponential behavior of the attenuation and a dominant magnetic character of the interaction; thus, the effect is strongly dependent on the g factor. Two limiting theories exist for the description of the deorientation effect. On one side, based on the theory of Abragam and Pound [33], first applied to deorientation in [34], the hyperfine interaction is described within a time-dependent perturbation framework and a rapidly changing hyperfine field. The second description is based on a static perturbation assuming a stable electron configuration, e.g., [23,24,35,36]. Within the second approach, one assumes a broad distribution of hyperfine frequencies whose superposition leads to the approximately exponential decay of the attenuation factors as observed in experiment. For this ansatz, it is required that the lifetimes of the electronic states are long compared to the nuclear state mean lifetime. The interaction is then described by attenuation factors averaged over the frequency distribution. From the physics point of view, a Gaussian distribution would be preferred, but a Lorentzian distribution is often used for mathematical simplicity. While the fluctuating character was used in earlier work, most investigations show strong evidence for the static approach, e.g., [23,36,37], and more recently, e.g., [42]. This description using a static interaction with a broad distribution of hyperfine frequencies is used in our work to parametrize the attenuation. It will be shown that with the introduced procedure it should be possible to measure relative g factors within an isotopic chain by determining differential attenuation coefficients using a plunger device. This method and applications will be presented in detail in a forthcoming paper [38].

To find the necessary correction factor, we started with the well-known angular distribution function following the convention of Rose and Brink [39]:

$$\begin{aligned} W(\Theta) &= \sum_{k \text{ even}, k \leq 4} R_k B_k Q_k P_k(\cos(\Theta)) \\ &= \sum_{k \text{ even}, k \leq 4} A_k P_k(\cos(\Theta)) \end{aligned}$$

with R_k taking into account the spin and multipolarity of the transition, B_k related to the alignment based on the m state

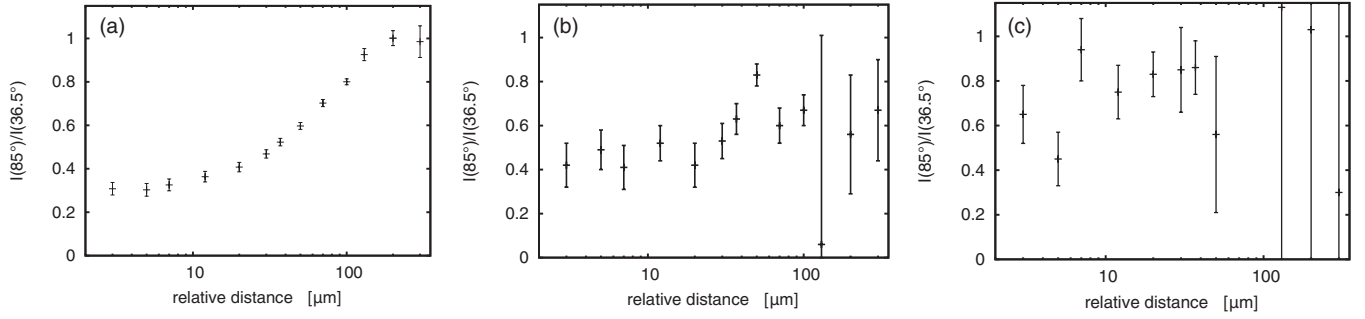


FIG. 6. The intensity ratios of the unshifted components at 85° and 36.5° of (a) the $2_1^+ \rightarrow 0_1^+$ transition, (b) the $4_1^+ \rightarrow 2_1^+$ transition and (c) the $2_2^+ \rightarrow 2_1^+$ transition.

population after the reaction and Q_k referring to the effects due to the finite solid angle of the Ge detectors [40].

We calculated the angular correlation using the Winther–de Boer code [41] for $d = 0$, i.e., $t = 0$, and for each solid angle of the particle detector $d\Omega_p$ that depends on the distance between target and stopper. The calculated correlation corresponds to the initial alignment of the excited nucleus. In the following, these calculated angular correlation parameters are called $A_k^{\text{coul}}(d = 0, d\Omega_p)$.

For further analysis a time-dependent factor has to be taken into account, the so-called attenuation factor $G_k(t)$:

$$W(t, \Theta) = \sum_{k \text{ even}, k \leq 4} R_k B_k Q_k G_k(t) P_k(\cos(\Theta))$$

thus,

$$\begin{aligned} W(d, \Theta) &= \sum_{k \text{ even}, k \leq 4} R_k B_k Q_k G_k(d) P_k(\cos(\Theta)) \\ &= \sum_{k \text{ even}, k \leq 4} A_k(d) P_k(\cos(\Theta)). \end{aligned}$$

This factor accounts for the fact that data are taken for different target-stopper distances and γ rays that are emitted from nuclei at different positions behind the target show a different alignment due to the deorientation effect. The alignment of the stopped nuclei emitting the γ ray at rest is assumed to remain unchanged in the stopper material [24].

Hence, to investigate the deorientation effect, we fitted the angular correlation

$$W(d, \Theta) = A_0(d) + A_2(d)P_2(\cos(\Theta)) + A_4(d)P_4(\cos(\Theta)) \quad (2)$$

to the data.

Examples for fitted angular correlations of the unshifted component at different distances are presented in Fig. 7(a). The angular correlations are normalized with respect to $A_0(d) = 0$ so that a comparison between different distances is possible. The increasing deorientation with time is clearly visible. In Fig. 7(b), shifted and unshifted components for the distance $d = 70 \mu\text{m}$ are shown. The detection angles for the shifted component were corrected for the angular aberration [30] due to the relativistic kinematics of the reaction. The difference in the angular correlations of the components is striking, i.e., due to the shorter interaction time, the angular correlation of the shifted component is less perturbed. In RDDS experiments, the ratio between both components is essential and should depend only on the lifetime. Other effects that influence this ratio have to be eliminated or corrected for.

Time-differential attenuation coefficients $G_k(d)$ are determined by comparing the angular distribution parameters at each distance with the parameters for the initial alignment at $d = 0$:

$$G_k(d) = \frac{A_k^{\text{exp}}(d)}{A_k^{\text{coul}}(d = 0, d\Omega_p)} \quad (3)$$

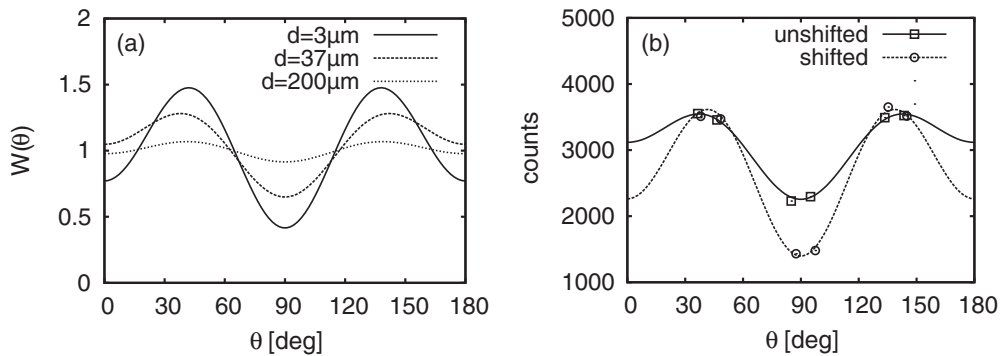


FIG. 7. (a) The normalized fitted particle- γ angular correlations of the unshifted component for the distances $d = 3, 37, 200 \mu\text{m}$. (b) The measured intensities and fitted angular correlations of the shifted (\circ and dashed line) and unshifted component for the distance $d = 70 \mu\text{m}$.

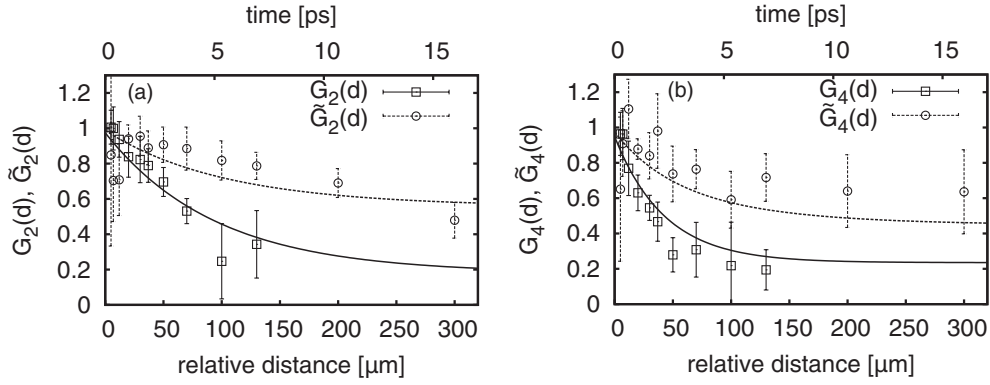


FIG. 8. The experimentally determined attenuation coefficients $G_k(d)$ and $\tilde{G}_k^{(\tau)}(d)$: (a) for $k = 2$ and (b) for $k = 4$. The fit was performed simultaneously using Eq. (5) for $G_k(d)$ and Eq. (7) for $\tilde{G}_k^{(\tau)}(d)$.

since the difference in these quantities is only due to the change in alignment.

The calculated angular correlation for $d = 0 \mu\text{m}$ was also used to normalize the data for the shortest distance $d = 3 \mu\text{m}$. Due to an accidentally missing efficiency calibration for the 90° clover detectors, the relative efficiency between the different detectors had to be determined differently. We decided to use the calculated intensities to normalize the shortest distance at which the alignment does not change significantly compared to the initial alignment. Thereby, we extracted the efficiencies for rings 3 and 4. Within error, this assumption does not have a major influence on the calculated attenuation factor. However, for the determined parameters, we added a systematic error. The distance $d = 3 \mu\text{m}$ was not taken into account for the determination of the attenuation parameters.

We parametrized $G_k(d)$ using the static approach, as discussed in [18,24,42],

$$G_k(t) = \alpha_k + (1 - \alpha_k) \cdot \exp(-\Gamma_k \cdot t) \quad (4)$$

equivalent to

$$G_k(d) = \alpha_k + (1 - \alpha_k) \cdot \exp\left(-\frac{\Gamma_k(d - d_0)}{v}\right). \quad (5)$$

We added an offset parameter d_0 since we measured only relative not absolute distances. The hard-core values α_k reflect the fact that hyperfine interactions of a static electron configuration cannot completely destroy the nuclear alignment. The parameters Γ_k are the widths of the Lorentzian describing the average of the precession frequencies, discussed in more detail in [18,24]. These Γ_k depend on the magnetic moment of the excited state and a time parameter C_k , e.g., [42],

$$\Gamma_k = \frac{|g|}{C_k}. \quad (6)$$

Since atomic (electron) configurations are the same for an isotopic chain (same chemical element), C_k is assumed to be constant for a given proton number, hence parametrizing the hyperfine interaction. Thus, by measuring the “strength” of the hyperfine interaction for one isotope, the determination of relative g factors within the isotopic chain is possible, or, with the knowledge of one g factor, the determination of the

magnitude [not the sign, see Eq. (6)] of g factors for the other isotopes. To perform these measurements, it is required that the velocity v/c of the isotope of interest is the same as for the calibration isotope in order to have a comparable distribution of charge states after the reaction. The beam charge state and the thickness of the target foil do not play a role as long as the chosen target material is sufficiently thick to assure that charge-state equilibrium is reached. The minimum thickness at beam energies as used in this work is around a few tenths of mg/cm^2 [24] and should be taken for granted in measurements of the type described here.

The transitions corresponding to the unshifted component belong to an exact interaction time t assuming a frozen alignment in the stopper material, while for the shifted radiation the interaction times vary between 0 and t . Thus, the attenuation factors for the shifted component have to be averaged by means of the decay function; the resulting formula is [24,43]

$$\tilde{G}_k^{(\tau)}(d) = \frac{\int_0^d G_k(x - d_0) \frac{1}{v\tau} \exp\left(-\frac{x-d_0}{v\tau}\right) dx}{\int_0^d \frac{1}{v\tau} \exp\left(-\frac{x-d_0}{v\tau}\right) dx}. \quad (7)$$

To determine the parameters α_k and Γ_k that describe the attenuation $G_k(d)$, the data extracted from the unshifted and shifted component were fitted simultaneously using Eq. (5) for the unshifted and Eq. (7) for the shifted component. Since the mean lifetime τ is needed for the shifted component, we started with the literature value for the lifetime, determined our deorientation-corrected lifetime τ and put the newly determined lifetime back in the attenuation parameter $\tilde{G}_k^{(\tau)}$. This two-step iteration turned out to be sufficient for an accurate deorientation correction. The results of the simultaneous fits are shown in Fig. 8, for $G_2(d)$, $\tilde{G}_2^{(\tau)}(d)$ in Fig. 8(a), for $G_4(d)$, $\tilde{G}_4^{(\tau)}(d)$ in Fig. 8(b). The distances $d = 200 \mu\text{m}$ and $d = 300 \mu\text{m}$ were not taken into account for the unshifted component since in these cases, no reasonable angular correlations were determined. For the distance $d = 450 \mu\text{m}$, the statistics are too poor to determine angular correlations for one of the components. The results for the attenuation parameters are given in Table I.

The large uncertainty on the attenuation factors can be reduced using more detection angles for the determination of

TABLE I. The determined parameters for the differential attenuation coefficient $G_k(d)$. For the calculation of the parameters C_k describing the strengths of the hyperfine interaction in the Ru isotopes, the g factor $g(2_1^+) = 0.47(3)$ [44] (another recently measured value is $g(2_1^+) = 0.41(3)$ [45]) was used.

	$k = 2$	$k = 4$
α_k	0.18(11)	0.24(13)
Γ_k [1/ps]	0.142(31)	0.314(110)
C_k [ps]	3.3(8)	1.5(5)

the angular correlation. Especially, the determined hard-core values are not reliable since missing data on larger distances and the large errors do not allow a reasonable determination of these values. With the recently measured g factor for the 2_1^+ state of $g = 0.47(3)$ [44] (another recently measured value is $g(2_1^+) = 0.41(3)$ [45]), one can calculate the parameters describing the hyperfine interaction strength in the Ru isotopes using Eq. (6) to $C_2 = 3.3 \pm 0.8$ ps and $C_4 = 1.5 \pm 0.5$ ps.

After determining $G_k(d)$, we calculated the correction factors $\alpha_{\text{deor}}(d, \Theta)$ for the shifted component for every distance and ring using

$$\alpha_{\text{deor}}(d, \Theta) = \frac{W^{\text{US}}(d, \Theta)}{W^{\text{SH}}(d, \Theta)}. \quad (8)$$

After correction for the deorientation effect, the normalized sum of shifted and unshifted component is constant within the error, see Fig. 9.

V. RESULTS

To extract lifetimes, data are analyzed by considering the in-flight decay probability $P = \frac{I^{\text{SH}}}{(I^{\text{SH}} + I^{\text{US}})}$ and applying the decay function in absence of feeding $P(t) = 1 - \exp(-\lambda t)$ with $\lambda = \frac{1}{\tau}$. Since the beam energy corresponds to only about 85% of the Coulomb barrier we primarily excited the first 2^+ state at $E = 652$ keV. The feeding due to two-step Coulomb excitation is negligible and is taken into account in the systematic error. A

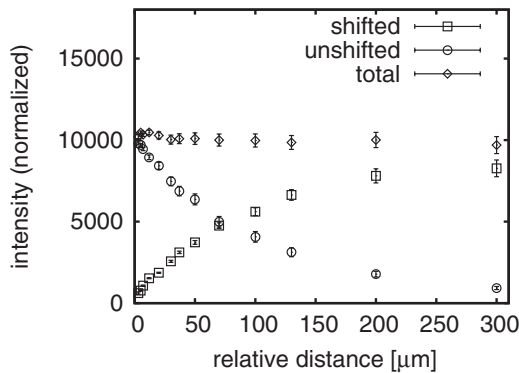


FIG. 9. The intensities of the shifted (\square) and unshifted (\circ) components of the $2_1^+ \rightarrow 0_1^+$ transition and the total number of counts $I^{\text{total}} = I^{\text{SH}} + I^{\text{US}}$ (\diamond) after the correction for deorientation. The total number of counts is constant within the error as expected (compare to Fig. 5).

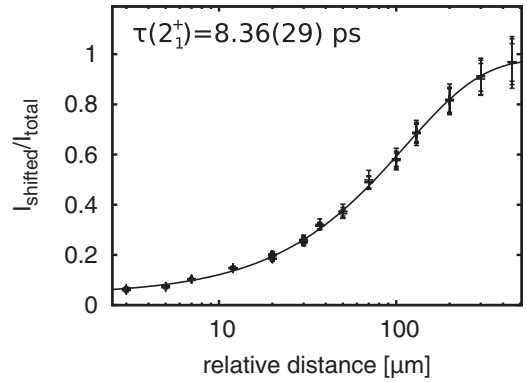


FIG. 10. Lifetime determination for the 2_1^+ state at $E = 652$ keV giving $\tau(2_1^+) = 8.36(29)$ ps. The different data points correspond to the four different rings 1, 2, 5, and 6. The fit was performed using Eq. (9). The distance is on a logarithmic scale.

scaling factor a and an offset parameter d_0 due to the minimum distance between target and stopper where electrical contact occurs are introduced so that the fitting function is given by

$$P(d) = a \cdot \left(1 - \exp\left(-\frac{d - d_0}{v\tau}\right) \right) \quad (9)$$

with the mean velocity of the excited ^{98}Ru nuclei $v = 13.49(18)$ $\mu\text{m}/\text{ps}$ and an offset d_0 of about $d_0 = 8(1)\mu\text{m}$, which was checked against the distance calibration for the NYPD.

For the ratio between the intensity of the shifted component and sum of the intensities of shifted and unshifted components, the corrections for the difference in efficiency for shifted and unshifted energies, Lorentz boost and deorientation were taken into account. Normalization and corrections due to the different solid angles of the particle detector are not necessary since they are the same for numerator and denominator.

The result for the 2_1^+ state is shown in Fig. 10. We analyzed the rings separately to get the adopted lifetime value of $\tau = 8.36(29)$ ps, which includes a systematic error of 2%. Figure 10 shows all data and shows the curve corresponding to the final result.

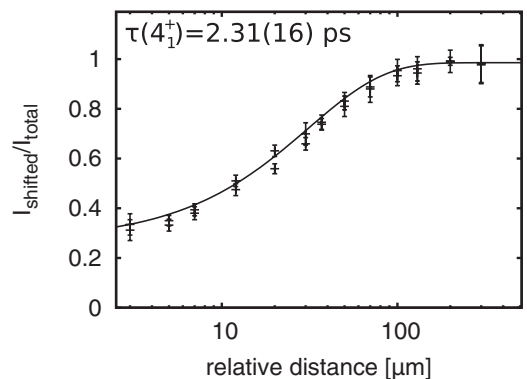


FIG. 11. Lifetime determination for the 4_1^+ state at $E = 1397$ keV giving $\tau(4_1^+) = 2.31(16)$ ps. The different data points correspond to rings 1 and 6. The fit was performed using Eq. (9). The distance is on a logarithmic scale.

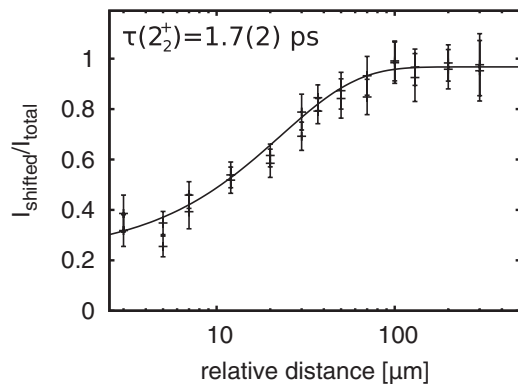


FIG. 12. Lifetime determination for the 2_2^+ state at $E = 1414$ keV giving $\tau(2_2^+) = 1.7(2)$ ps. The different data points correspond to rings 1 and 6. The fit was performed using Eq. (9). The distance is on a logarithmic scale.

For the 2_2^+ and 4_1^+ states a correction due to deorientation was not necessary. Within error, there was no visible effect in the normalized total number of counts as well as in the ratio $I(85^\circ)/I(41.5^\circ)$ as shown in Figs. 6(b) and 6(b). The results for the lifetimes are shown in Fig. 11 for the 4_1^+ state with $\tau(4_1^+) = 2.31(16)$ ps and in Fig. 12 for the 2_2^+ state with $\tau(2_2^+) = 1.7(2)$ ps. For both states, we used only rings 1 and 6 in the analysis. The states and corresponding decays to the 2_1^+ state are close in energy and were barely separable in rings 2 and 5, which correspond to the clover leaves closer to 90° , and therefore have a smaller Doppler Shift. The intensity for $d = 450$ μm was not determined since statistics were not sufficient at this largest measured distance.

In Table II, the results are summarized. For comparison, the literature values [7,8,10] are listed as well.

VI. DISCUSSION

As can be seen in Table II, we significantly reduced the uncertainty on the lifetimes of the 2_1^+ , 4_1^+ , and 2_2^+ states. The determined reduced transition probability for the $2_1^+ \rightarrow 0_1^+$ transition is $B(E2; 2_1^+ \rightarrow 0_1^+) = 31.0(17)$ W.u. This is in agreement with a weakly collective vibrational character, as

expected for a nucleus close to the $N = 50$ shell closure with an $R_{4/2} = E(4_1^+)/E(2_1^+)$ value of $R_{4/2} = 2.1$. The systematics of the $B(E2; 2_1^+ \rightarrow 0_1^+)$ values is shown for the Ru isotopes as well as for the $N = 54$ isotones in Figs. 13(a) and 13(b). Both systematics show similar behavior: For the Ru isotopes, an increase of the transition strength from the near-shell nucleus ^{96}Ru to midshell nuclei illustrates the growth of collectivity; For the $N = 54$ isotones with $40 \leq Z \leq 48$, an increase with proton number from Zr and a decrease when approaching the $Z = 50$ shell closure is observed that clearly indicates the valence maximum between the Sr/Zr and Sn shell closures at $Z = 44$. In Figs. 13(c) and 13(d) the $B_{4/2}$ values are shown for the Ru isotopes and $N = 54$ isotones, respectively. Both reflect the enhanced collective character going to midshell. For the Ru isotopes, the maximum of $B_{4/2}$ at ^{98}Ru points at its spherical nature. Its vibrational character is enhanced compared to ^{96}Ru , due to larger collectivity, and with $B_{4/2} = 1.86$ it is the best candidate for a spherical vibrator in the Ru isotopic chain. It is worth noting that ^{94}Zr has a relatively weak $B(E2; 2_1^+ \rightarrow 0_1^+)$ value indicating the subshell closure at $Z = 40$, but has a weakly collective $B_{4/2}$ value. This emphasizes the limits of interpretations based on ratios instead of absolute numbers.

In [9], an IBM-1 fit was performed using the Hamiltonian $H = \epsilon n_d + \kappa Q \cdot Q$ with $Q = (s^\dagger \tilde{d} + d^\dagger s) + \chi (d^\dagger \tilde{d})^{(2)}$ resulting in the parameters $\epsilon = 0.682$ MeV, $\kappa = -0.02$ MeV, and $\chi = -0.51$. The agreement between theory and experiment regarding the energies is discussed in [9]. Up to the two-phonon triplet and for the yrast levels, the calculation reproduces the experimental values. For the three-phonon states, however, the IBM fails to describe level energies and decay behavior likely reflecting effects of the limited valence space, which is not inherent to the IBM. In this work, the calculated yrast levels are compared with respect to the $E2$ transition strengths connecting the ground state band levels using the parameters from [9]. The effective boson charge was adjusted so that the calculated $B(E2; 2_1^+ \rightarrow 0_1^+)$ value agrees with the experimental one. In Table III, the theoretical and experimental transition strengths are compared.

The IBM calculation gives $B_{4/2} = 1.5$, slightly lower than the experimentally determined one of $B_{4/2} = 1.86(16)$. However, the experimental value agrees well with the prediction

TABLE II. Our results in comparison with previously published data from [7,8,10]. A systematic error of 2% is added to the statistical error. The branching ratios and multipole mixing ratios needed to calculate the transition strengths for the depopulating 2_2^+ transitions are taken from [46]. Due to an uncertain transition strength for the $2_2^+ \rightarrow 0_2^+$ transition there are two $B_{4/2}$ values given in [10].

J^π	E_{level} [keV]	E_γ [keV]	τ [ps] (NNDC)	τ [ps] (this work)	$B(E2)$ [W.u.] (NNDC)	$B(E2)$ [W.u.] (this work)	$B_{4/2}$ (NNDC)	$B_{4/2}$ (this work)
2_1^+	652	652	7.9 (1.2) [8] 9.2 (1.7) [7]	8.36(29)	32 (5) [8] 28 (5) [7]	31 (1)	0.35 (11) [8] 1.4 (3) [7] 1.7 (6), 2.0 (7) [10]	1.86 (16)
4_1^+	1397	745	11 (2) [8] 3.3 (4) [7]	2.31(16)	12 (3) [8] 40 (5) [7]	57.6 (40)		
2_2^+	1414	761 1414	1.7 (6) [8]	1.7(2)	45 (16) [8] 1.0 (4) [8]	47 (5) 1.05 (42)		

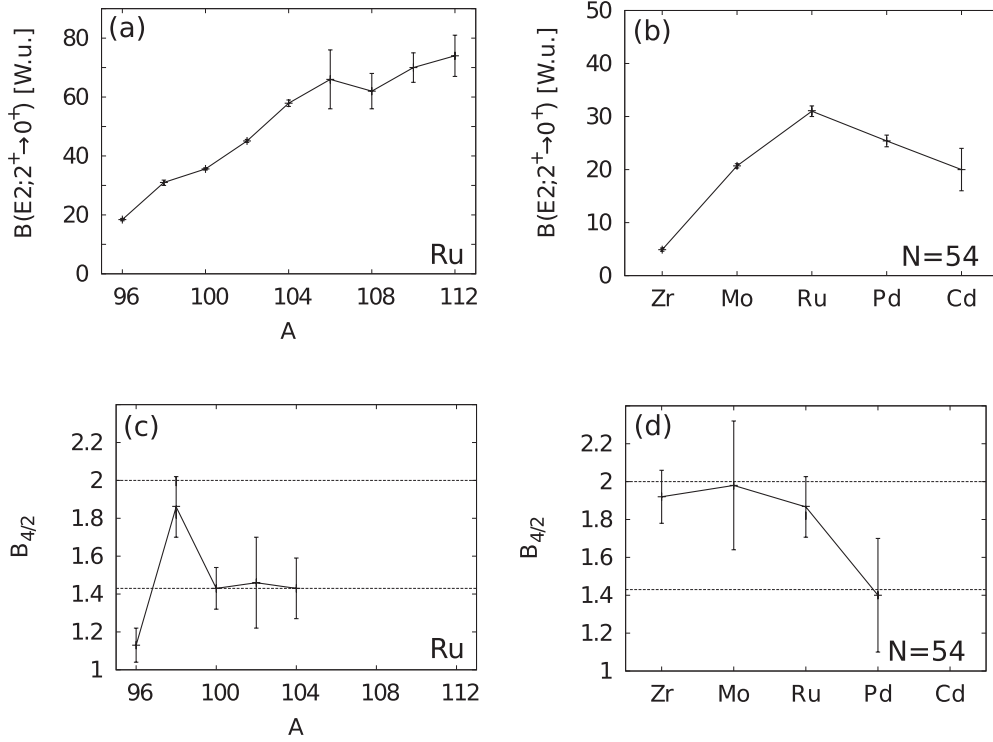


FIG. 13. Top: Systematics of the $B(E2)$ strengths of the $2_1^+ \rightarrow 0_1^+$ transition for the Ru isotopes with $52 \leq N \leq 68$ (a) and the $N = 54$ isotones with $40 \leq Z \leq 48$ (b). Bottom: Systematics of the $B_{4/2}$ value for the Ru isotopes with $52 \leq N \leq 68$ (c) and the $N = 54$ isotones with $40 \leq Z \leq 48$ (d). Data are taken from [47–49].

in the geometrical limit not taking into account the finite number of bosons. The transitions between the higher-spin yrast states taken from [8] show strong disagreement with the IBM-1 calculations. However, weak $E2$ transitions between the 6_1^+ and 4_1^+ , and 8_1^+ and 6_1^+ are a well known feature in this mass region, investigated, e.g., in [50]. On the other hand, a systematic error in the measurement published in [8] would be conceivable since the strength of the $4_1^+ \rightarrow 2_1^+$ transition was determined to be much weaker than in this work. As the main focus of this work was the determination of the $B_{4/2}$ value, the higher-spin structure of ^{98}Ru is not further discussed here, but will be explored in an forthcoming publication where

the results from the $\gamma\gamma$ angular correlation experiment are presented [16].

VII. SUMMARY

The lifetimes of the 2_1^+ , 2_2^+ , and 4_1^+ state in ^{98}Ru were measured via the RDDS method using Coulomb excitation in inverse kinematics. The newly determined lifetimes have smaller uncertainties and resolve the disagreement in the published lifetimes of the 4_1^+ state that were subject to discussions in literature due to a $B_{4/2}$ value smaller than 1. The newly extracted $B_{4/2}$ value for ^{98}Ru is $B_{4/2} = 1.86(16)$ and hints at a vibrational character of the low-energy excitations in ^{98}Ru . To determine the lifetime of the 2_1^+ state, the crucial correction for the deorientation effect was performed via the measured perturbation of the distance-dependent particle- γ angular correlations.

Provided suitable lifetimes, i.e., lifetimes in the sensitive region of the RDDS method and on the order of the deorientation time, are present, the simultaneous measurement of deorientation and lifetime in inverse kinematics has major advantages. In particular, it is suitable for radioactive beam experiments and it allows the determination of relative g factors within isotopic chains due to the magnetic character of the hyperfine interaction. For the measurement of g factors, calibration data on the hyperfine strengths within an isotopic chain is needed as long as no theoretical description is available. It is also important to find the

TABLE III. Comparison between the experimental and theoretical $E2$ transition strengths. The $B(E2)$ values are calculated using the parameters from [9]. The values for the $6_1^+ \rightarrow 4_1^+$ and $8_1^+ \rightarrow 6_1^+$ transitions are taken from [8].

J^π	$E_{\text{level}}^{\text{exp}}$ [keV]	$E_{\text{level}}^{\text{theo}}$ [keV]	E_γ^{exp} [keV]	E_γ^{theo} [keV]	$B(E2)^{\text{exp}}$ [W.u.]	$B(E2)^{\text{theo}}$ [W.u.]
2_1^+	652	661	652	661	31 (1)	31
2_2^+	1414	1367	761	706	47 (5)	45
			1414	1367	1.05(42)	0.01
4_1^+	1397	1362	745	701	57.6(40)	47
6_1^+	2222	2101	824	739	12.9(15)	46
8_1^+	3126	2873	904	772	2.5(4)	30

optimum v/c for such g -factor measurements on an isotopic chain.

ACKNOWLEDGMENTS

This work was supported by the US Department of Energy under grant no. DE-FG02-91ER-40609. One author (D.R.) thanks the German Academic Exchange Service (DAAD)

for financial support. We thank P. Petkov, A. Stuchbery, N. Benzcer-Koller, G. Kumbartzki, K.-H. Speidel, M. Hackstein, T. Thomas, A. Blazhev, and M. Elvers for fruitful discussions. Furthermore, we thank the operators Jeffery Ashenfelter, Walter Garnett, Salvatore DeFrancesco, Anazoba Ezeokoli and Francisco Lopez for excellent beam conditions.

-
- [1] F. Iachello and A. Arima, *Ann. Phys. (NY)* **99**, 253 (1976).
 [2] F. Iachello and A. Arima, *The Interacting Boson Model* (Cambridge University Press, Cambridge, 1987).
 [3] M. Büyükkata, P. Van Isacker, and İ. Uluer, *J. Phys. G* **37**, 105102 (2010).
 [4] A. Frank, C. E. Alonso, and J. M. Arias, *Phys. Rev. C* **65**, 014301 (2001).
 [5] K. Pomorski, L. Próchniak, K. Zajac, S. G. Rohoziński, and J. Srebrny, *Phys. Scr.*, **T 88**, 111 (2000).
 [6] K.-H. Kim, A. Gelberg, T. Mizusaki, T. Otsuka, and P. von Brentano, *Nucl. Phys. A* **604**, 163 (1996).
 [7] S. Landsberger, R. Lecomte, P. Paradis, and S. Monaro, *Phys. Rev. C* **21**, 588 (1980).
 [8] B. Kharraja *et al.*, *Phys. Rev. C* **61**, 024301 (1999).
 [9] R. B. Cakirli *et al.*, *Phys. Rev. C* **70**, 044312 (2004).
 [10] E. Williams *et al.*, *Phys. Rev. C* **74**, 024302 (2006).
 [11] J. R. Terry, V. Werner, Z. Berant, R. J. Casperson, R. F. Casten, A. Heinz, G. Henning, R. Luttker, E. A. McCutchan, J. Qian, B. Shoraka, E. Williams, and R. Winkler, *Proceedings of the 13th International Symposium on Capture Gamma-Ray Spectroscopy and Related Topics, Cologne, Germany 25–29 Aug. 2008*, edited by J. Jolie, A. Zilges, N. Warr, and A. Blazhev, AIP Conf. Proc. 1090 (AIP, 2009), p. 337.
 [12] W. Rother *et al.*, *Nucl. Instrum. Methods Phys. Res. A* **654**, 196 (2011).
 [13] T. K. Alexander and J. S. Forster, in *Advances in Nuclear Physics*, edited by M. Baranger and E. Vogt (Plenum Press, New York, 1978), Vol. 10, p. 197.
 [14] A. Linnemann, Ph.D. thesis, University of Cologne, 2005 (unpublished).
 [15] D. Radeck, M. Albers, C. Bernards, L. Bettermann, A. Blazhev, C. Fransen, S. Heinze, J. Jolie, and D. Mücher, *Nucl. Phys. A* **821**, 1 (2009).
 [16] D. Radeck *et al.* (in preparation).
 [17] R. J. Sturm and M. W. Guidry, *Nucl. Instrum. Methods Phys. Res. A* **138**, 345 (1976).
 [18] P. Petkov, A. Dewald, A. Gelberg, G. Böhm, P. Sala, P. von Brentano, and W. Andrejtscheff, *Nucl. Phys. A* **589**, 341 (1995).
 [19] A. E. Stuchbery, *Nucl. Instrum. Methods Phys. Res. A* **385**, 547 (1997).
 [20] A. Dewald, S. Harrissopoulos, and P. von Brentano, *Z. Phys. A* **334**, 163 (1989).
 [21] G. Böhm, A. Dewald, P. Petkov, and P. von Brentano, *Nucl. Instrum. Methods Phys. Res. A* **329**, 248 (1993).
 [22] P. Petkov, *Nucl. Instrum. Methods Phys. Res. A* **349**, 289 (1994).
 [23] H. R. Andrews, R. L. Graham, J. S. Geiger, J. R. Beene, O. Häusser, D. Ward, and D. Horn, *Hyp. Int.* **4**, 110 (1978).
 [24] G. Goldring, in *Heavy Ion Collision*, Vol. 3, edited by R. Bock (North-Holland Publishing Company, Amsterdam, 1982).
 [25] J. Billowes, *Hyp. Int.* **30**, 265 (1986).
 [26] N. J. Stone *et al.*, *Phys. Rev. Lett.* **94**, 192501 (2005).
 [27] R. Krücken, *J. Res. Natl. Inst. Stand. Technol.* **105**, 53 (2000).
 [28] R. Krücken, *Proceedings of the International Conference on Applications of Accelerators in Research and Industry*, CAARI, 2000 (AIP, New York, 2001), p. 319.
 [29] C. W. Beausang *et al.*, *Nucl. Instrum. Methods Phys. Res. A* **452**, 431 (2000).
 [30] D. Pelte and D. Schwalm, in [24].
 [31] N. J. Stone, J. R. Stone, and P. Jonsson, *Hyp. Int.* **197**, 29 (2010).
 [32] H.-D. Betz, *Rev. Mod. Phys.* **44**, 465 (1972).
 [33] A. Abragam and R. V. Pound, *Phys. Rev.* **92**, 943 (1953).
 [34] I. Ben Zvi, P. Gilad, M. Goldberg, G. Goldring, A. Schwarzschild, A. Sprinzak, and Z. Vager, *Nucl. Phys. A* **121**, 592 (1968).
 [35] R. Brenn, H. Spehl, A. Weckherlin, H. A. Doubt, and G. van Middelkoop, *Z. Phys. A* **281**, 219 (1977).
 [36] J. Billowes, *Hyp. Int.* **30**, 265 (1986).
 [37] G. Goldring, K. Hagemeyer, N. Benzcer-Koller, R. Levy, Y. Lipshitz, B. Richter, Z. Shkedi, Y. Wolfson, and K. H. Speidel, *Hyp. Int.* **5**, 283 (1977).
 [38] G. Ilie *et al.* (in preparation).
 [39] H. J. Rose and D. M. Brink, *Rev. Mod. Phys.* **39**, 306 (1967).
 [40] J. Barrette, G. Lamoureux, and S. Monaro, *Nucl. Instrum. Methods* **93**, 1 (1971).
 [41] A. Winther and J. De Boer, California Institute of Technology, Technical Report, 18 November, 1965; in *Perspectives in Physics Series: Coulomb Excitation*, edited by K. Alder and A. Winther (Academic Press, New York, 1966).
 [42] A. E. Stuchbery and N. J. Stone, *Phys. Rev. C* **76**, 034307 (2007).
 [43] A. E. Stuchbery, P. F. Mantica, and A. N. Wilson, *Phys. Rev. C* **71**, 047302 (2005).
 [44] M. J. Taylor *et al.*, *Phys. Rev. C* **83**, 044315 (2011).
 [45] S. K. Chamoli *et al.*, *Phys. Rev. C* **83**, 054318 (2011).
 [46] B. Singh and Z. Hu, *Nucl. Data Sheets* **98**, 335 (2003).
 [47] D. Radeck *et al.*, *Phys. Rev. C* **80**, 044331 (2009).
 [48] G. Audi, A. H. Wapstra, and C. Thibault, *Nucl. Phys. A* **729**, 337 (2003).
 [49] G. Audi and A. H. Wapstra, *Nucl. Phys. A* **595**, 409 (1995).
 [50] K. P. Lieb *et al.*, *Phys. Rev. C* **63**, 054304 (2001).